Supplementary Information Appendix

Patient	1	2	3	4		5	6	7	8
Session	1	2	3	4	5	6	7	8	9
Age	23	40	49	24	25	31	40	23	39
Gender	male	male	male	female	female	female	male	male	male
Weight (kg)	73	88	62	45	45	97	64	110	70
Recording duration (min)	41	59	90	79	53	46	50	48	40
Duration of Wakefulness / Anesthesia (sec)	332 (limited by length of noise-free wakefulness recording)	480	300 (limited by length of noise-free wakefulness recording)	465 (limited by length of noise-free anesthesia recording)	480	480	177 (limited by rapid anesthetic descent)	390 (limited by rapid anesthetic descent)	480
Stimuli	40Hz CT	40Hz CT	40Hz CT; target + 3 other words	40Hz CT; target + 6 other words	40Hz CT; target + 5 other words	40Hz CT; target + 4 other words	40Hz CT; target + 4 other words	40Hz CT; target + 4 other words	40Hz CT; target + 4 other words
Behavioral Task	no	no	yes	yes	yes	yes	yes	yes	yes
Anesthetic Agents	propofol; fentanyl; midazolam	propofol; remifentanil	propofol	propofol	propofol	propofol	propofol	propofol	propofol
Auditory region label (Fig. 3)	--	pmHG1 (L)	--	pmHG2 (R)	midHG (R)	pmHG3 (L) and pmHG4 (R)	N/A (grid)	--	pPT & aSTG (both L)
No. of auditory responsive units	0	0	0	1x SU / 2x MU	5x SU / 3x MU	10x SU / 7x MU	N/A (grid)	N/A (no microwire data)	1x MU
Total No. of units from wires in/around Heschl's Gyrus	0	0	0	1x SU / 8x MU	6x SU / 3x MU	11x SU / 14x MU	N/A (grid)	N/A (no microwire data)	3x SU / 4x MU
Regions targeted by most medial contacts	RAH, RA, RMF, LAH, LA, LMF	RA, RAH, REC, RHSC, RPHG, RMF, LA, LAH, LHSC, LMF	LA, LAH, LMTO, LOp, LOm	RMF, REC, RMH, RA, RSTG, RAC, RpSMA, LEC-LPHG, LAH, LAC, LpSMA	RAH, RaSTG, RmSTG, RmP, RpSMA, RdAC, RmSFG, RMF, RmOF, RFP, RMTO	LAH, RAH, LA, RA, LEC, REC, LHSC, RHSC, LMH, LPHC, RPHC	RFTG, RBTOS, RPBTS, RIFS, RMFS, RFSG	LAF, LdAC, LvaCING, LSF, LpGaCING, LMH, LEC, RdAC, RpGaCING, RSF	LOF, LAI, LMI, LSI, LPI, LSTG, LPHG, RA, REC, RMH
Seizure Onset Zone	RAH	Predominantly middle RHSC, but also middle/ lateral LHSC	LAH	Right temporal / frontal lobes	Right superior frontal gyrus	Left superior temporal gyrus near LHSC	Poorly defined. Probably in Rt anterior temporal lobe	LAF/ LpGaCING	Seizure onset zone unclear

SI Table S1. Data acquisition details

Data acquisition details for the nine recording sessions included in this study. Rows (top to bottom) show patient number, session number, age, gender, weight, recording duration, auditory stimuli, behavioral task, anesthetic agents, BIS monitoring, label of auditory region, number of auditory responsive units, targeted regions, and seizure onset zone. Sessions 1 – 6 and 8 - 9 involved depth electrodes whilst session 7 involved a subdural grid and subdural strips. Sessions 4 and 5 involved the same patient who was re-admitted with new electrode locations due to inconclusive clinical results from her first hospital admission. Abbreviations: 40Hz CT = 40Hz click-train; SU = single neuronal unit; MU = multi neuronal unit; L=left hemisphere; R = right hemisphere; pmHG = posteromedial Heschl's gyrus; midHG = middle Heschl's gyrus; pPT = posterior planum temporale; aSTG = anterior superior temporal gyrus; AH = anterior hippocampus; A = amygdala; MF = medial frontal; MTO = medial temporal occipital junction; Op = occipital lobe, posterior aspect; Om = occipital lobe, medial aspect; EC=entorhinal cortex; HSC=Heschl's gyrus; MH=middle hippocampus; STG = superior temporal gyrus; AC = Anterior cingulate cortex; pSMA = pre-Supplementary Motor Area; PHG = parahippocampal gyrus; mSTG = superior temporal gyrus – middle part; mP = parietal lobe – medial aspect; dAC = dorsal anterior cingulate; mSFG = middle superior frontal gyrus; mOF = medial orbitofrontal; FP = frontal pole; MC = middle cingulate gyrus; PHC = parahippocampal cortex; FTG = frontotemporal grid; BTOS = basal temporal occipital strip; PBTS = post-basal temporal strip; IFS = inferofrontal strip; MFS = middle frontal strip; FSG = frontal small grid; AF = anterior frontal; vaCING = ventral anterior cingulate; pGaCING = pre-genual anterior cingulate; SF = superior frontal

a

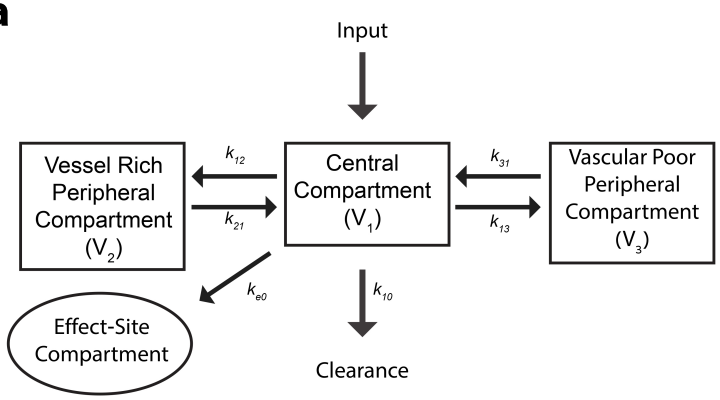

b

$$\frac{dC_e}{dt} = k_{e0} \times \left(\frac{m_1}{V_1} - C_e\right)$$

$$\frac{dm_{clearance}}{dt} = k_{10} \times m_1$$

$$\frac{dm_2}{dt} = k_{12} \times m_1 - k_{21} \times m_2$$

$$\frac{dm_3}{dt} = k_{13} \times m_1 - k_{31} \times m_3$$

$$\frac{dm_1}{dt} = input - \frac{dm_2}{dt} - \frac{dm_3}{dt} - \frac{dm_{clearance}}{dt}$$

$$V_1 = 0.228\,\mathrm{L\,kg^{-1}} \times PntWeight$$

$$V_2 = 0.463\,\mathrm{L\,kg^{-1}} \times PntWeight$$

$$V_3 = 2.893\,\mathrm{L\,kg^{-1}} \times PntWeight$$

$$k_{10} = 0.119\,\mathrm{min^{-1}}$$

$$k_{12} = 0.112\,\mathrm{min^{-1}}$$

$$k_{13} = 0.042\,\mathrm{min^{-1}}$$

$$k_{21} = 0.055\,\mathrm{min^{-1}}$$

$$k_{31} = 0.0033\,\mathrm{min^{-1}}$$

$$k_{e0} = 0.26\,\mathrm{min^{-1}}$$

Fig. S1. Modelling time dynamics of propofol concentration

(a) Three compartment pharmacokinetic model ("Marsh Model" (1)) used to estimate propofol concentration in the effect-site compartment (analogue to the brain) of each patient at any given moment (Fig. 1c and Supplementary Fig. 2) given the known rate of propofol infusion ("Input"), and parameters. (b) Actual parameter values used, based on patient's weight ("PntWeight") (2–4). Note that while V_2 and V_3 do not explicitly appear in the model equations, they ensure that concentrations in the various compartments (= mass / volume) are equal during equilibrium. The effector site concentrations estimated by this model at the moment of LOR ranged between 0.49 – 2.8 μg/mL (for patients who did not receive adjuvant agents). Similar (albeit slightly higher) estimates were obtained when using the Schnider model (not shown), ranging between 0.91 – 4.2 μg/mL. Such variability in effector site concentrations at LOR is in line with literature (5–9).

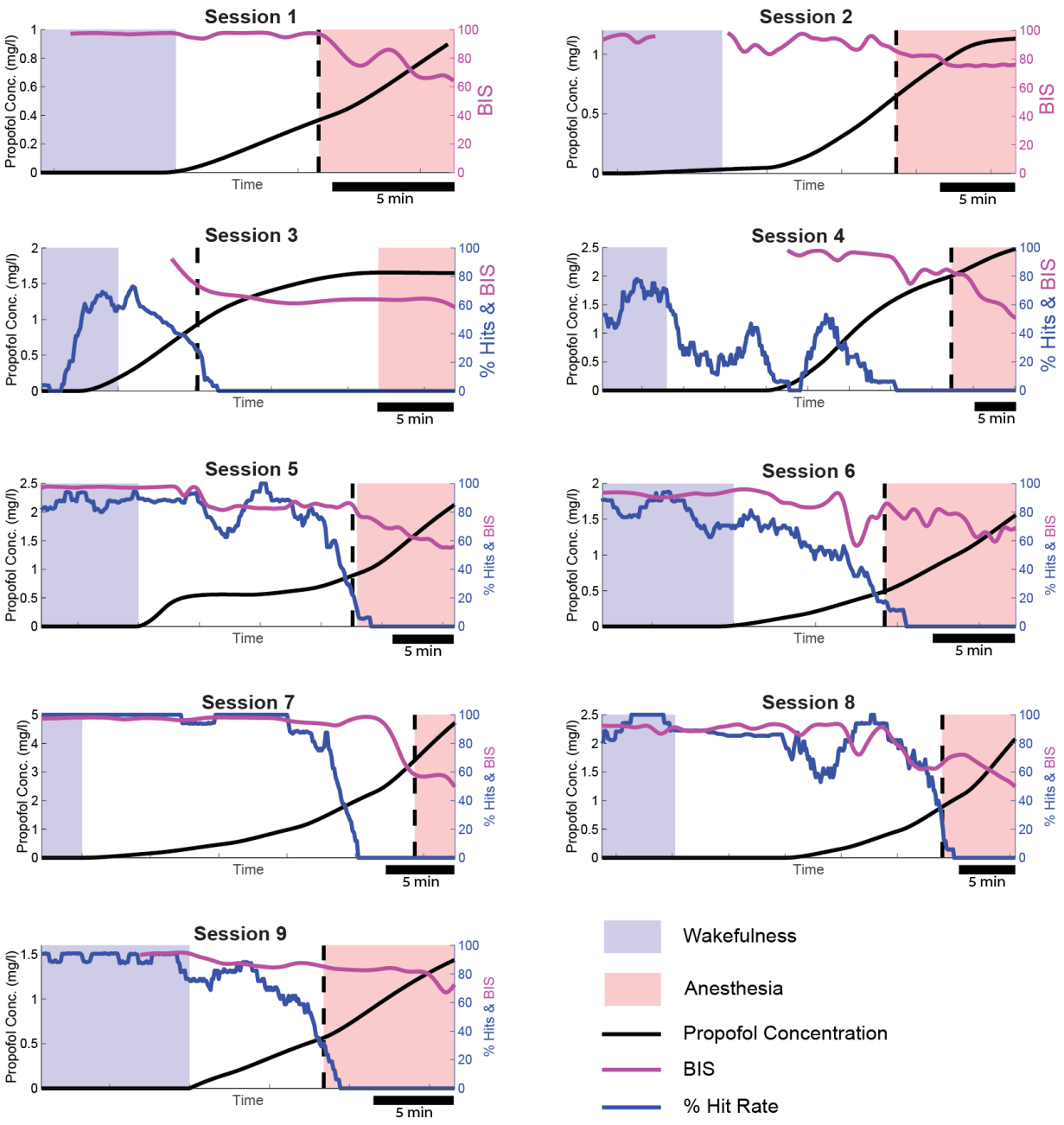

Fig. S2. Time dynamics of anesthesia, behavior, and BIS in each experimental session

Superimposed time dynamics in each experimental session (subpanels) showing estimated effector site (brain) propofol concentrations (black trace and y-axis on left), BIS values (purple trace and y-axis on right), and behavioral performance (blue trace and y-axis on right, proportion of successful button presses). The vertical dashed black line marks loss of responsiveness (the final time the patient successfully pressed the button to the target word). The behavioral performance ("%Hits") curve is calculated as a moving window average over approximately 16 trials (≈150 sec), and therefore may overshoot the loss of responsiveness line. Blue and red shading mark periods of wakefulness and anesthesia, respectively, used

for analysis of auditory responses (whenever possible, about 8 minutes of light anesthesia with BIS>50, Methods). In session 3, the anesthesia period for analysis occurred 12 minutes after LOR due to technical issues before that time.

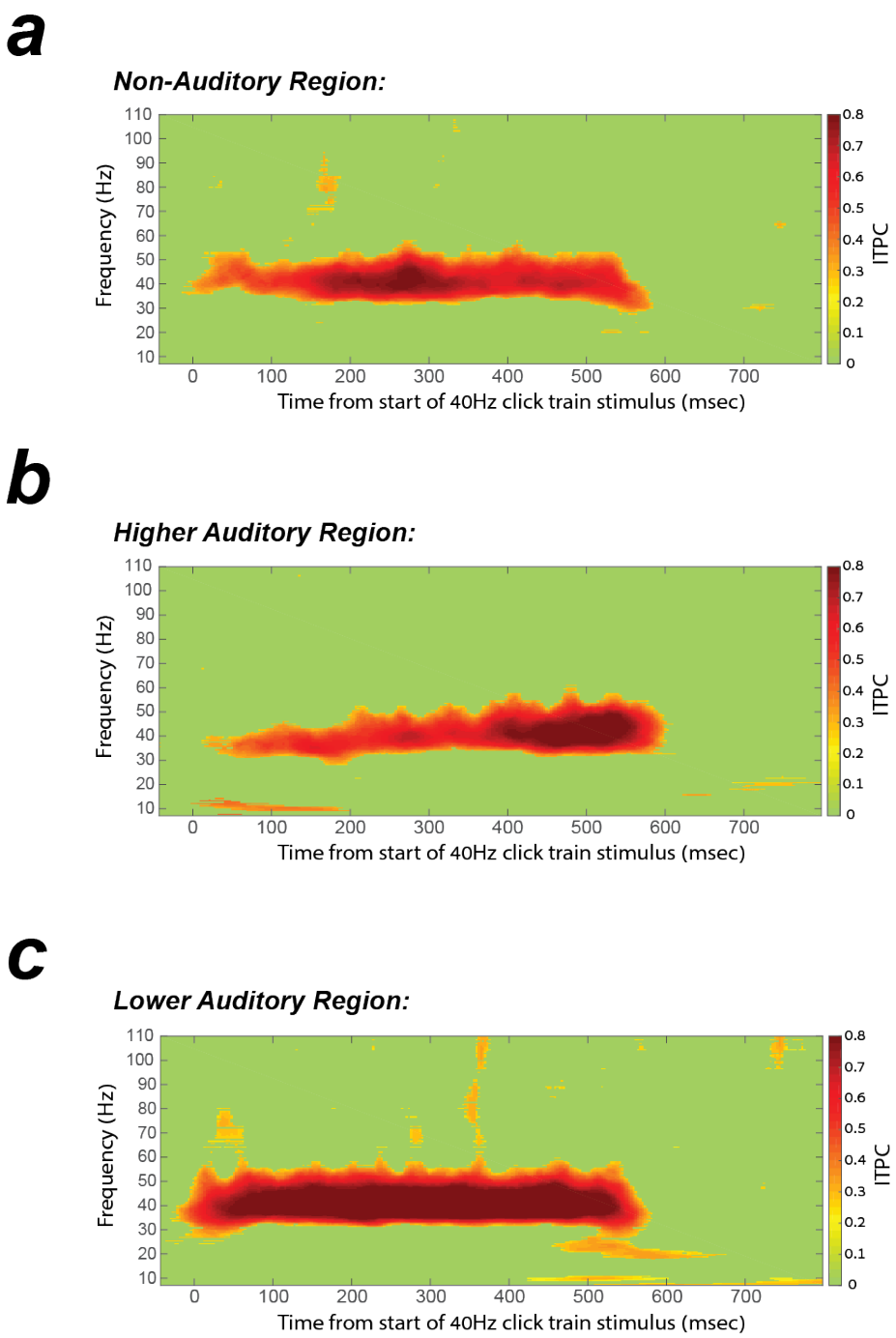

Fig. S3: 40-Hz click trains elicit significant Inter Trial Phase Coherence (ITPC) at stimulation frequency

Wideband ITPC spectrogram of responses to 40-Hz click trains during wakefulness in (a) a representative iEEG macro-electrode in association cortex (session 5, 64 trials), in (b) a representative LFP microwire electrode in higher auditory region (session 5, 64 trials), and in (c) a representative LFP microwire electrode in the PAC (session 6, 75 trials).


Session 1
n=48
Awake:
Anesthesia:
Session 2
n=77
Awake:
Anesthesia:
Session 3
n=40
Awake:
Anesthesia:
Session 4
n=88
Awake:
Anesthesia:
Session 5
n=74
Awake:
Anesthesia:
Session 6
n=88
Awake:
Anesthesia:
Session 7
n=63
Awake:
Anesthesia:
Session 8
n=57
Awake:
Anesthesia:
Session 9
n=77
Awake:
Anesthesia:
ITPC
1.0
0.9
0.8
0.7
0.6
0.5
0.4
0.3
0.2
ns
Median ITPC per Session
Median ITPC
p = 0.004
Session 1, n=17
Session 2, n=48
Session 3, n=33
Session 4, n=77
Session 5, n=66
Session 6, n=68
Session 7, n=35
Session 8, n=53
Session 9, n=24
Wakefulness
Anesthesia

Fig. S4: Attenuation of iEEG 40-Hz click-train responses outside primary auditory cortex in individual sessions

Each subpanel shows auditory responses in all iEEG macroelectrodes in each experimental session separately (see Supplementary Table 1 for details). Each circular patch shows a specific iEEG electrode and its color (colorbar) denotes Inter Trial Phase Coherence at 40 Hz (ITPC) during wakefulness (top) and during anesthesia (bottom), as shown on a standard flat cortical surface. Bottom-right panel shows median ITPC per session in wakefulness vs. anesthesia for iEEG contacts showing responses during either state.

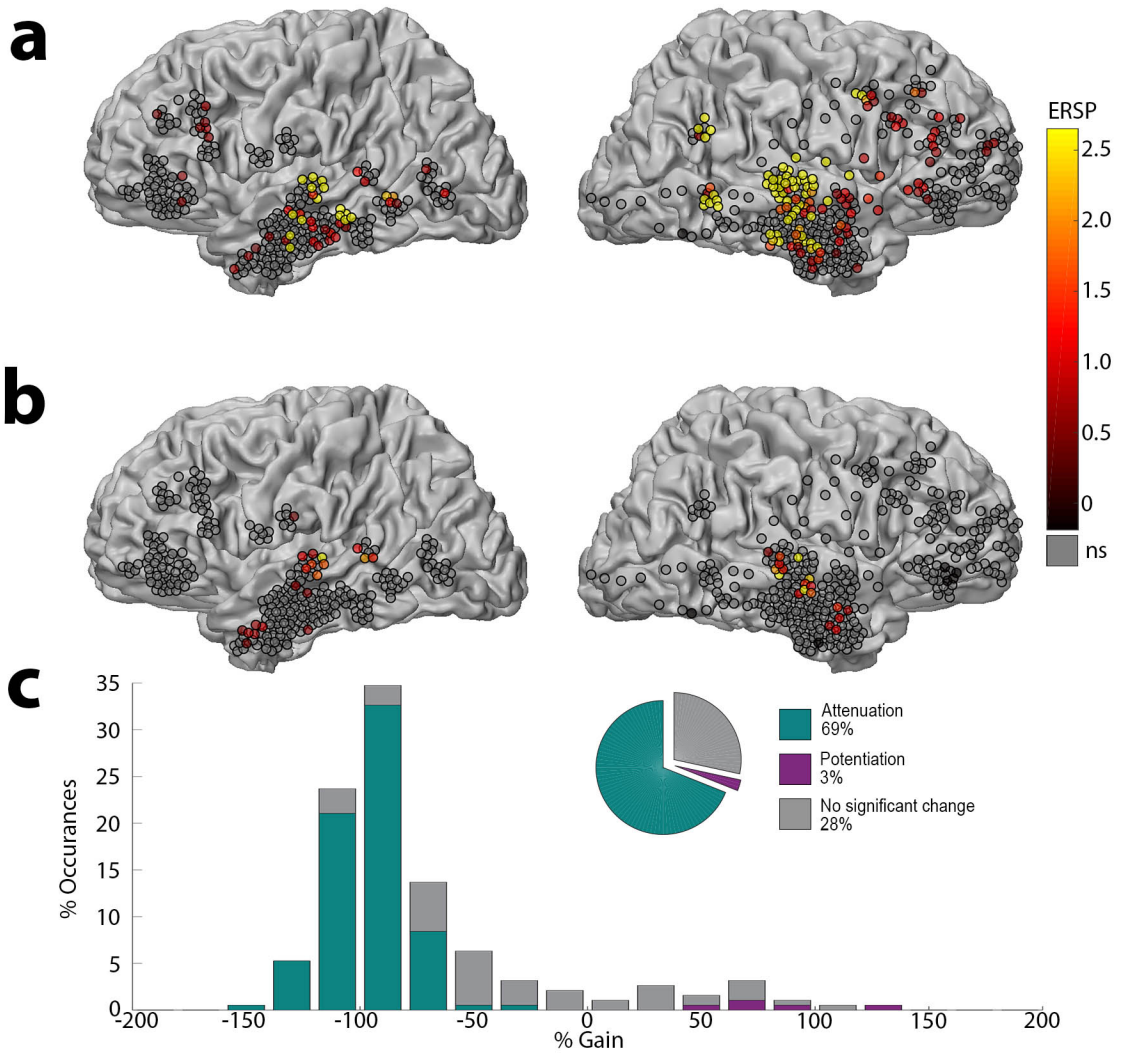

Fig. S5: Event-Related Spectral Power (ERSP) in iEEG responses to 40-Hz click trains during wakefulness and anesthesia

(a) ERSP at each iEEG electrode (n = 612 in 9 sessions) in response to 40-Hz click trains during wakefulness, as shown on a grey-white matter boundary surface as seen from lateral view. (b) Same during anesthesia. Note that anesthesia-induced LOC disrupts iEEG responses outside auditory cortex as was seen when quantifying the response via ITPC. (c) Quantification of the 190 iEEG contacts showing significant responses during either wakefulness or anesthesia, revealing that 69% of these electrodes undergo significant attenuation under anesthesia, compared to only 3% showing potentiation.

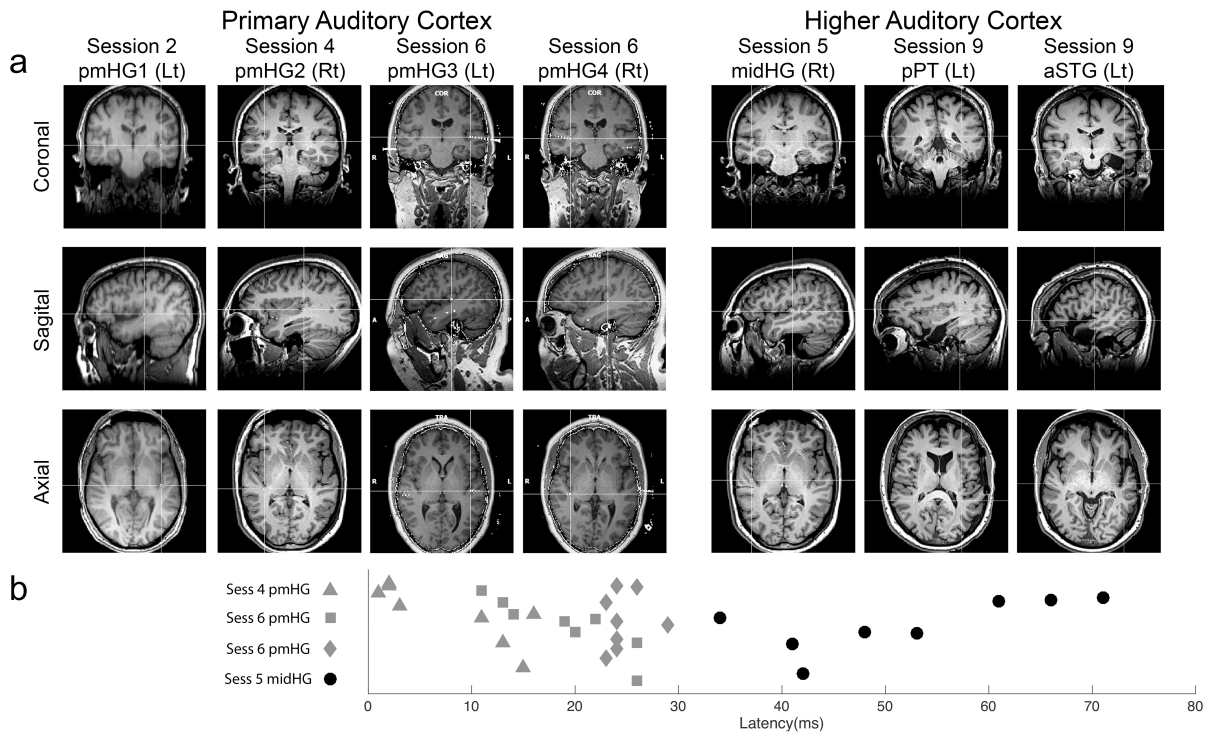

Fig. S6. Classification of auditory regions to PAC vs. higher-order based on anatomy and response latency to 40-Hz click trains.

(a) Anatomical T1 weighted MRI scans centered on each microwire region, confirming locations within Heschl's gyrus (PAC), or nearby locations (Higher Auditory Cortex). (b) Latency plots for each microwire with sufficient inter-trial coherence to allow latency to be measured. All PAC microwires showed latency < 30ms (mean 17 ± 9 ms), whilst all midHG microwires were > 30ms (mean 52 ± 13 ms). Lt = left hemisphere, Rt = right hemisphere, pmHG = posteromedial Heschl's gyrus, midHG = middle Heschl's gyrus, pPT = posterior planum temporale, aSTG = anterior superior temporal gyrus.

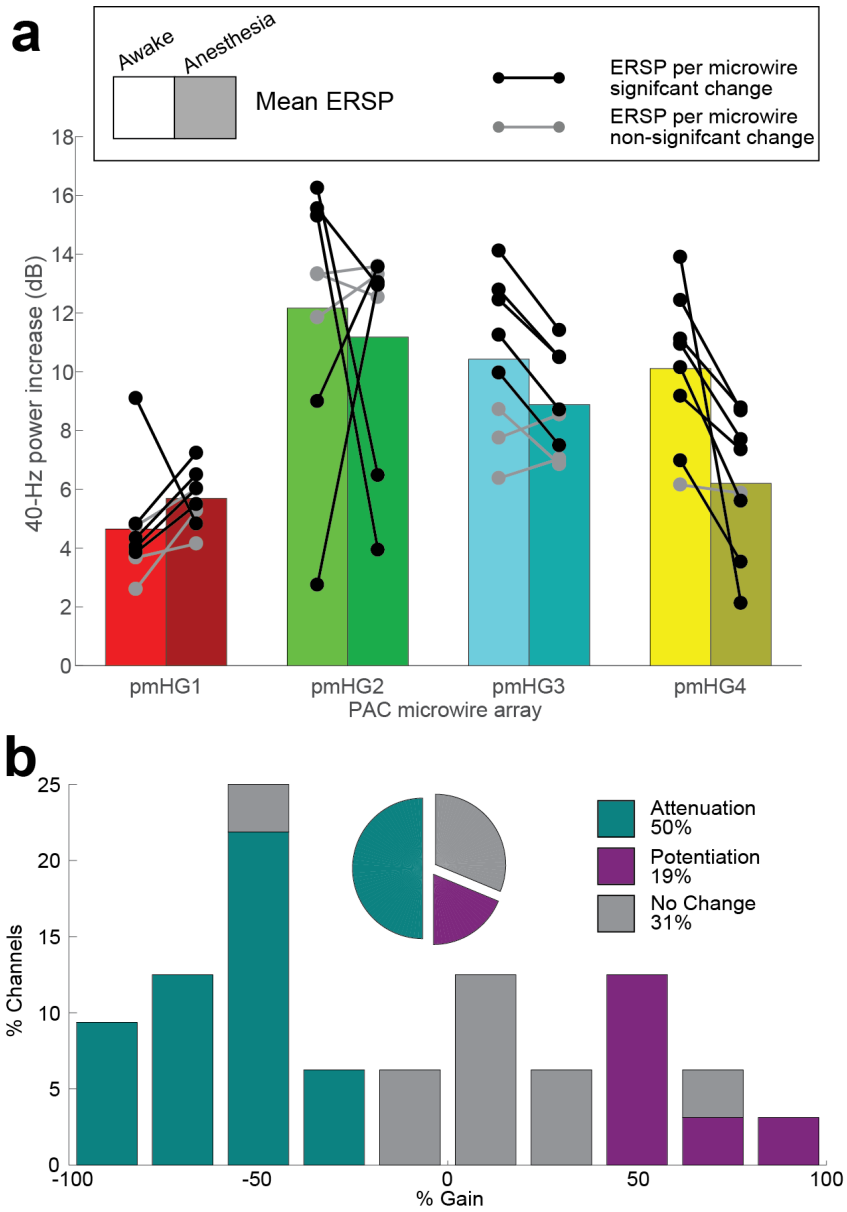

Fig. S7. Event-Related Spectral Power (ERSP) in primary auditory cortex to 40Hz click-trains during wakefulness and anesthesia

(a) Event Related Spectral Power (ERSP) at 40Hz in response to click trains across all 32 PAC microwires (circles), and averaged per region (bars), during wakefulness (left bar, bright colors) and anesthesia (right bar, dull colors). PAC microwires showing significant changes ($p<0.05$ Wilcoxon rank sum) are in black, whilst those not showing significant change are marked in grey. (b) Histogram of gain in ERSP under anesthesia in all 32 PAC microwires, divided according to significant attenuation, significant potentiation, and no significant change ($p>0.05$, Wilcoxon rank sum) under anesthesia. As was the case for ITPC (Fig. 3C), LFP responses in PAC are relatively preserved, a profile that is significantly different than observed for iEEG power changes in association cortex (Supplementary Figure 5).

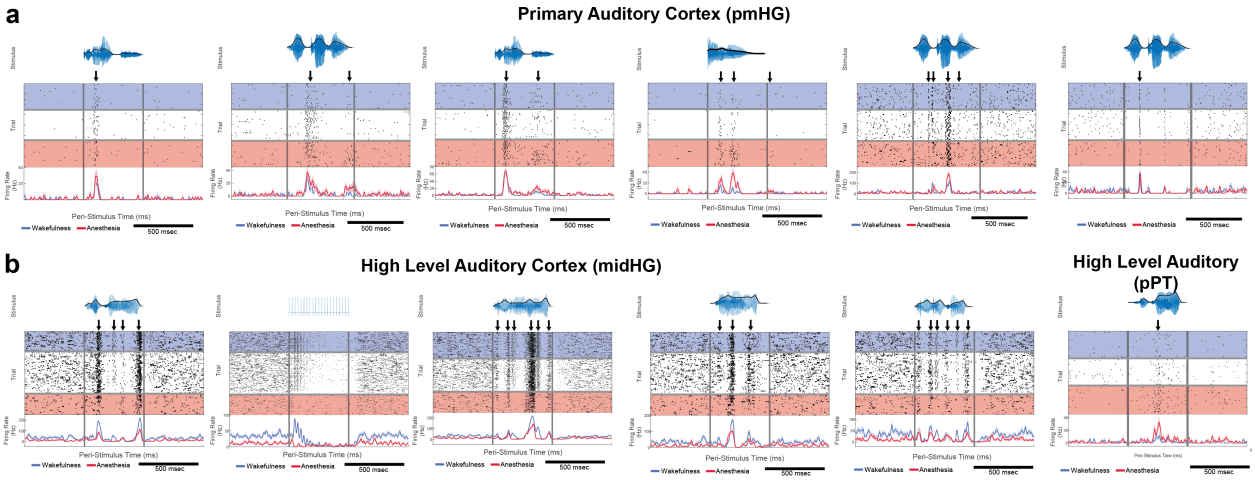

Fig. S8. Additional examples of neuronal unit spike responses to words upon anesthesia-induced LOC.

(a) Example raster plots and PSTHs of single-neuron spike responses to words in PAC. Each subpanel shows a different stimulus (click-train or word, waveform on top in blue and its power envelope in black). In each subpanel, rows (top to bottom) mark individual trials during deepening propofol anesthesia. Black arrows indicate identified response components. Blue shading and PSTH time-course, wakefulness; Red shading and PSTH time-course, anesthesia. Vertical gray lines mark stimulus onset and offset. (b) Same as (a) for high-level auditory cortex. Each subpanel shows the response of one neuron to one stimulus and may include one (e.g. in 1st panel) or more (other panels) response components.

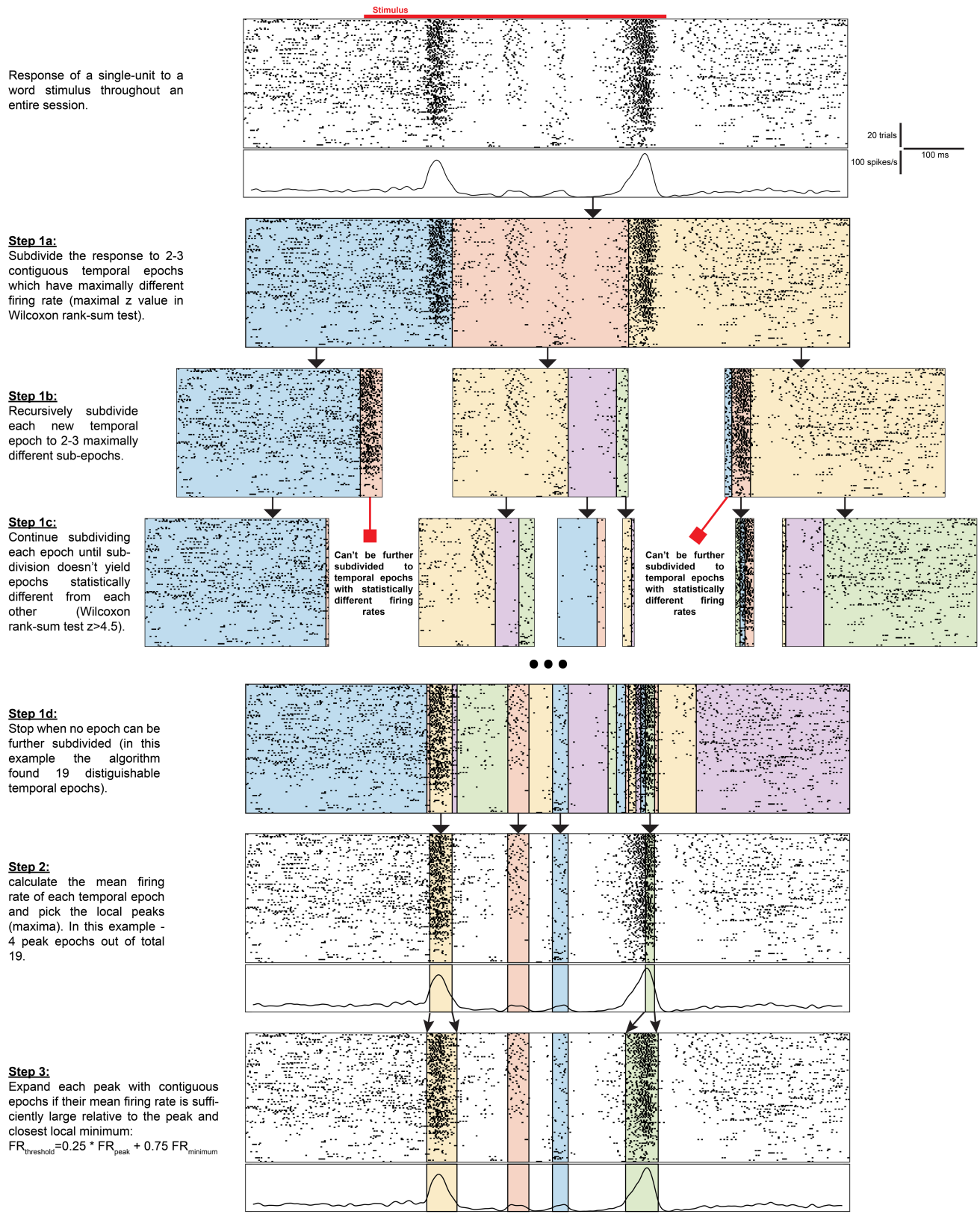

Fig. S9. Response detection algorithm flowchart

SI Automatic response detection algorithm

Raster and peri-stimulus time histograms (PSTH) were produced for each neuronal unit in response to each word (see Supplementary Fig. 8 for examples). Instantaneous firing rate traces (all PSTHs below raster plots) were calculated by smoothing the binary spike trains with a Gaussian kernel (σ = 5 ms). For each raster, periods of increased firing were identified as "response components" (black arrows in Supplementary Fig. 8) using an automatic detection algorithm (Supplementary Fig. 9). The algorithm works by identifying firing rate peaks, statistically distinguished (WRST z statistic>4.5) from their surroundings, in the response raster (including all trials: wakefulness, transition and anesthesia). The algorithm first divides the temporal interval of the response to two or three smaller contiguous temporal epochs with maximally statistically different firing rates (using WRST, Supplementary Fig. 9, step 1a). Each temporal epoch is then recursively subdivided to smaller and smaller temporal epochs (Supplementary Fig. 9, step 1b) until no further subdivision yields epochs with statistically different firing rates (WRST z statistic>4.5, Supplementary Fig. 9, step 1c). Then, the algorithm calculates the mean firing rate for each temporal epoch and identifies the local peaks among the temporal epochs (Supplementary Fig. 9, step 2). Each peak singles out an individual response component. Temporal epochs contiguous with the peak-epoch are then combined with it if they have sufficiently large firing rate (relative to the peak and adjacent local minimum), exceeding the following threshold (Supplementary Fig. 9, step 3):

$$FR_{Threshold} = 0.25 * FR_{peak} + 0.75 * FR_{closest\ local\ minimum}$$

A single unit responding to a few isolated acoustic events (e.g. phonemes) within a single word stimulus could therefore have one or more response components (Supplementary Fig. 8 and 9), and the firing rate (total spikes) of each such component was compared separately between wakefulness and anesthesia.

Supplementary References and Notes

1. B. Marsh, M. White, N. Morton, G. N. Kenny, Pharmacokinetic model driven infusion of propofol in children. *Br. J. Anaesth.* **67**, 41–8 (1991).
2. A. R. Absalom, V. Mani, T. De Smet, M. M. R. F. Struys, Pharmacokinetic models for propofol- Defining and illuminating the devil in the detail. *Br. J. Anaesth.* **103**, 26–37 (2009).
3. S. Cascone, G. Lamberti, G. Titomanlio, O. Piazza, Pharmacokinetics of Remifentanil: a three-compartmental modeling approach. *Transl. Med. @ UniSa* **7**, 18–22 (2013).
4. ALARIS, *Arsena PK Syringe Pump Manual* (Alaris Medical Systems, 2004).
5. H. Iwakiri, *et al.*, Individual Effect-Site Concentrations of Propofol are Similar at Loss of Consciousness and at Awakening. *Anesth. Analg.* **100**, 107–110 (2005).
6. R. Ní Mhuircheartaigh, C. Warnaby, R. Rogers, S. Jbabdi, I. Tracey, Slow-wave activity saturation and thalamocortical isolation during propofol anesthesia in humans. *Sci. Transl. Med.* **5**, 208ra148 (2013).
7. E. a Mukamel, *et al.*, A transition in brain state during propofol-induced unconsciousness. *J. Neurosci.* **34**, 839–45 (2014).
8. M. H. Davis, *et al.*, Dissociating speech perception and comprehension at reduced levels of awareness. *Proc. Natl. Acad. Sci. U. S. A.* **104**, 16032–16037 (2007).
9. G. G. Supp, M. Siegel, J. F. Hipp, A. K. Engel, Cortical hypersynchrony predicts breakdown of sensory processing during loss of consciousness. *Curr. Biol.* **21**, 1988–1993 (2011).